Parameterization of Vegetation Scattering Albedo in the *Tau-Omega* Model for Soil Moisture Retrieval on Croplands

Chang-Hwan Park [1*], Thomas Jagdhuber [2], Andreas Colliander [3], Johan Lee [1], Aaron Berg [4], Michael Cosh [5], Seung-Bum Kim [3], Yoonjae Kim [1], Volker Wulfmeyer [6]

[1] National Institute of Meteorological Sciences, Earth System Research Division, Korea Meteorological Administration (KMA), Jeju, Republic of Korea; johanlee07@korea.kr (J.L.); yoonjaekim@korea.kr (Y.K.)
[2] Microwaves and Radar Institute, German Aerospace Center (DLR), 82234 Weßling, Germany; Thomas.Jagdhuber@dlr.de
[3] Jet Propulsion Laboratory, California Institute of Technology, 4800 Oak Grove Drive, Pasadena CA91109, USA; andreas.colliander@jpl.nasa.gov; seungbum.kim@jpl.nasa.gov
[4] University of Guelph, Department of Geography, Environment and Geomatics, Guelph, ON, Canada; aberg@uoguelph.ca
[5] USDA ARS Hydrology and Remote Sensing Laboratory, Beltsville, MD, USA; michael.cosh@usda.gov
[6] Institute of Physics and Meteorology, University of Hohenheim, Stuttgart 70599, Germany; volker.wulfmeyer@uni-hohenheim.de
* Correspondence: ecomm77@gmail.com or chpark2@kma.go.kr; Tel.: +82-10-4206-2058

Abstract: An accurate radiative transfer model (RTM) is essential for the retrieval of soil moisture (SM) from microwave remote sensing data, such as the passive microwave measurements from the Soil Moisture Active Passive (SMAP) mission. This mission delivers soil moisture products based upon L-band brightness temperature data, via retrieval algorithms for surface and root-zone soil moisture, the latter is retrieved using data assimilation and model support. We found that the RTM based on the tau-omega (τ-ω) model, can suffer from significant errors over croplands (in average between -9.4K and + 12.0K for Single Channel Algorithm SCA; -8K and + 9.7K for Dual-Channel Algorithm DCA) if the vegetation scattering albedo (omega) is treated as a constant and the temporal variations are not accounted. In order to reduce this uncertainty, we propose a time-varying parameterization of omega for the widely established zeroth order radiative transfer τ-ω model. The main assumption is that omega can be expressed by a functional relationship between vegetation optical depth (tau) and the Green Vegetation Fraction (GVF). The validation was performed from 14 May to 13 December 2015 over 61 Climate Reference Network sites (SCRN) classified as croplands. The application of the proposed time-varying vegetation scattering albedo results in a consistent improvement for the unbiased root mean square error of 16% for SCA and 15% for DCA. The reduction for positive and negative biases was 45% and 5% for SCA and 26% and 12% for DCA, respectively. This indicates that vegetation dynamics on croplands are better represented by a time-dynamic single scattering albedo.

Keywords: soil moisture; scattering albedo; tau-omega model; allometry; vegetation fraction; vegetation water content; passive microwave remote sensing; SMOS; SMAP; AMSR-E

1. Introduction

The prediction of weather extreme events, such as heat waves and cold surges, is important in time spans from one week to several months (S2S: sub-seasonal to seasonal) [1]. However, existing weather and climate models still perform very poorly in the prediction for this time scale. This issue is known as the weather and climate prediction gap [4]. At this time scale, the initial conditions of atmosphere, land and ocean components affect the prediction skill. One of the important missing pieces in S2S predictions is the role of the land surface; in particular, soil moisture, which is the main variable transferring water and energy to atmosphere. Furthermore, soil moisture plays an important

role in cloud and precipitation formation emphasized in the recent modeling and land-atmosphere feedback studies [5–7]. Estimation of global soil moisture variability, particularly within the root zone, can be realized in a land surface model using data assimilation of remote sensing measurements [8]. Assimilation systems opens new possibilities to improve the accuracy and robustness of land surface models with microwave brightness temperature assimilated from satellite such as the SMAP mission [9–11] and SMOS mission [12–14]. For this purpose, accurate and realistic microwave radiative transfer modelling (RTM) is essential as an operator for simulating microwave brightness temperature (*Tb*). One of the uncertainty sources in microwave RTM is modelling of wave-canopy interaction, which is commonly represented with a zeroth-order RTM using vegetation optical depth (VOD) and single scattering albedo (omega) [15-17].

Currently, the SMAP baseline soil moisture algorithm (SCA, single channel algorithm) use an NDVI climatology-based VOD in its RTM [18]. The wavelength, or frequency, limits the penetration of electromagnetic waves through vegetation. At shorter the wavelengths there is less capacity it has to penetrate through the vegetation saturating the VOD at lower vegetation density. Longer wavelengths have the ability to capture VOD over wider range of the vegetation growth stages [19]. Therefore, low-frequency microwave measurements from L-band Radiometers such as SMAP and using algorithms such as Dual-Channel Algorithm, DCA [20] and Multi-Temporal DCA, MT-DCA [21] allows full penetration of wide variety of vegetation types.

In this study, we will investigate the improvement of the operational SMAP SCA and DCA algorithms by proposing a time-varying parameterization of omega for the two algorithms. Currently, both of the SMAP operational algorithms consider the scattering albedo as constant, e.g. value of 0.05, for cropland type, while in experimental algorithms such as the MT-DCA omega is varying in space but fixed over time domain of the retrieval period for SM and tau. An important difference between DCA and MT-DCA is whether omega is estimated by the cost function minimization along with tau and soil moisture. The main assumption in the minimization of the cost function of MT-DCA is that the temporal variability of scattering albedo is much larger than soil moisture and tau. However, the assumption of one fixed omega for each vegetation type domain may be invalid over heterogeneous surfaces and for fast growing crops. This heterogeneity issue ultimately adds to the uncertainty of soil moisture estimation using SCA, DCA and MT-DCA algorithms (e.g. [22]). In this study, we apply time- and space-varying omega that is synchronized with VOD and investigate whether a newly parameterized (time-varying vegetation scattering albedo) tau-omega (τ-ω) radiative transfer model based on SCA and DCA is able to simulate *Tb* more accurately over spatially and temporally heterogeneous croplands.

2. Methods

2.1. The τ-ω model of vegetated soil emission

The τ-ω model represents a zeroth order solution of the radiative transfer equation [17] and is a common basis of current passive microwave electromagnetic interaction modeling with vegetated soils at L-band. This model is also applied in the SMAP soil moisture retrieval algorithms [18]. It expresses the aggregated brightness temperature in the resolution cell over of view as follows [23]:

$$Tb^{land} = e_s\gamma T + (1-\omega)(1-\gamma)T + \gamma(1-e_s)(1-\omega)(1-\gamma)T \quad (1)$$

$$\text{where, } \gamma = \exp(-\tau/\cos\theta)$$

Tb^{land} is the brightness temperature, emitted from land surface; e_s is the soil emissivity; γ indicates the transmissivity of canopy which is determined by vegetation optical thickness τ at nadir incidence θ; T is the physical surface temperature, and ω is the single-scattering albedo, set to a constant of 0.05 ($\omega_{0.05}$) for croplands in the SMAP SCA. In this study, this approach is called the fixed-omega approach. The basis to estimate the value of τ (or VOD) has arguably improved from the NDVI-based τ used in SCA. In DCA and MT-DCA, τ or τ and ω are directly determined from

the polarimetric microwave L-band *Tb,* respectively. In this study, we focus on improving the scattering parameter ω, which is a constant in space and time for SCA and DCA and a constant in time for MT-DCA. In contrast, we by establish a spatially heterogeneous and temporally varying ω_{var} to account for the heterogeneity of vegetation scattering albedo in croplands and their dynamics. Owing to the varying omega, we differentiate this approach from the MT-DCA (multi-temporal dual channel algorithm) where omega is a time-constant value over the optimization period. The latter is retrieved from a model selection during multi-temporal optimization of the estimation of τ and permittivity [24].

2.2. New Parameterization of vegetation scattering albedo ω with GVF

In order to derive the temporally varying vegetation scattering albedo (ω) within the τ-ω model, we assume that omega can be derived based on a proportionality to the sub-grid scale vegetation fraction, Green Vegetation Fraction (*GVF*) [25].

$$\omega_{var} = (1 - GVF)\omega_0 + GVF\,\omega_{max} \tag{2}$$

Based on this assumption, the temporal variability of ω_{var} is determined by the temporal variability of the vegetation fraction GVF. With no vegetation scattering condition for the bare soil fraction (1-*GVF*), ω_0 becomes 0, which leads Eq. (2) to:

$$\omega_{var} = GVF\ \omega_{max} \tag{3}$$

2.3 Combining tau and omega via GVF

In this study, our hypothesis is that we can parametrize the 2-D (spatial) vegetation cover fraction (*GVF*) with the measured VOD via a power-law function. Firstly, VOD (or τ) can be expressed with a parameter *b* and the vegetation water content *VWC* [24],

$$\tau = b\,VWC \tag{4}$$

where b is a parameter related to the wavelength and vegetation structural characteristics. Now, we define the vegetation cover fraction with the vegetated area, A, per unit ground area.

$$GVF\ \ [m^2/m^2] = A\ [m^2]\ /1\ [m^2] \tag{5}$$

Studies in the past have established empirical relationships between above ground biomass (AGB) and tree height, H. The allometric relationship has been derived as AGB ~ H^2 for forest by [26, 27]. As vegetation grows, it typically increases in height (H) and covers a larger area (A). The height and area of vegetation can be related using allometric functions. Using allometric functions we express the 1-D height in terms of the 2-D area of the vegetation calculated with tree diameter D [28–30]. However, instead of using the ln(H)-ln(D^2) non-linear approach, we apply an H-D linear approach without violation of their physical units as shown in Eq (6),

$$H\ [m] = c \cdot \sqrt{A\ [m^2]} \tag{6}$$

where c is a non-dimensional factor related with environmental variables and model uncertainty from the proposed function [28]. In a recent study, total *VWC* in a SMAP grid was scrutinized in terms of volume and height of canopy by [31],

$$VWC = \rho_E \rho VH \tag{7}$$

where physical density of plant elements (ρ_E), density of canopy in plant elements (ρ), volume of vegetation (V), height of vegetation layer (H). In this study, we express V as a function of a (area of a plant element) and h (the unique thickness the unique thickness of the plant element):

$$V = a\,h \tag{8}$$

If all plant elements are homogeneous in a measured resolution cell, we can compute the vegetation area as shown in Eq. (9)

$$A = \sum_{i=1}^{N} a_i = \rho\, a, \tag{9}$$

where ρ is the number density of the plant elements.
Then we can get the volume of a plan element from A and h.

$$V = \frac{A}{\rho} h \tag{10}$$

Hence

$$VWC = \rho_E \cdot c \cdot A^{3/2} \cdot h \tag{11}$$

Then, we can express vegetation optical depth (τ) by putting Eq. (8) into Eq. (4) and using Eq. (6):

$$\tau = b\rho_E chGFV^{3/2} \tag{12}$$

Then, *GVF* can be expressed with tau, a vegetation canopy parameter b [m²/kg], a canopy environmental parameter including an uncertainty c [-] and unique parameters for a specific plant: ρ_E [kg/m3], and h [m], which are collectively expressed with the non-dimensional parameter γ. [-]:

$$GFV = \gamma\tau^{2/3} \tag{13}$$

This results in a new *GVF* [cm²/cm² or %] – τ [-] relationship. The new relationship is differentiated from the exponential function of LAI which can be estimated as tau or *VWC* via the approximated relation (τ = 0.5*LAI) [32] to estimate the vegetation fraction proposed by [33]. Chaubell et. al and Fernandez-Moran et. al ([34–36]) suggested that VOD is proportional to grass or crop height linearly. But the non-linearity between VOD - vegetation fraction turned out to be the power-law function with 2/3 exponent as shown in Eq. (13). Finally, without ancillary input, ω_{eff} can be derived as power-law function of tau based on Eq. (3) and (10) as following.

$$\omega_{eff} = \omega_{max} \cdot \gamma \cdot \tau^{2/3} \tag{14}$$

In the various studies [33–39], the constant or average ω ranged from 0.05 to 0.12. In this study, the ω_{max} (vegetation scattering albedo with no bare soil exposed in the SMAP grid) is empirically set to 0.1.

2.5 Experimental Results and Validation of Parameterization

In order to confirm the developed time-dynamic vegetation scattering albedo approach, we performed a validation process. The control cases (SCA1 and DCA1) are used for *Tb* simulation with in-situ SM which is the reference input as shown in Fig.1. In this step, the difference between the simulated and observed *Tb* is considered as the modelling mismatch (mainly ω in this study).

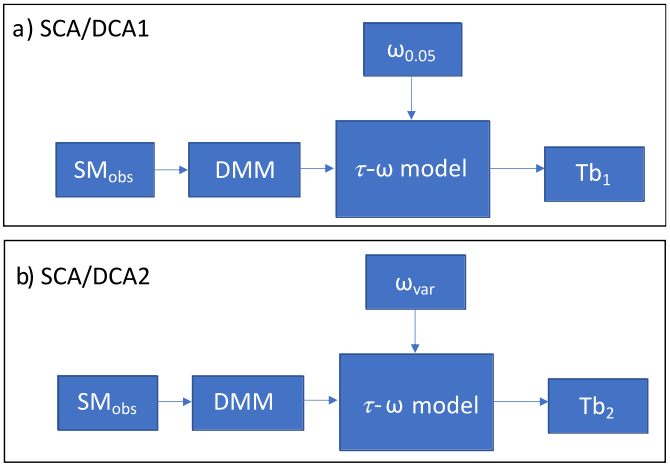

Fig.1 Simulation of brightness temperatures (*Tb*) using the a) classical τ-ω model with time-constant ω , b) time-varying parameterization of the τ-ω model with variable ω (DMM: dielectric mixing model)

Table.1 Experimental set up to validate the effect of time-varying vegetation scattering albedo ω in the τ-ω model.

Model	Simulation	Vegetation part		Soil part	
		τ	ω	DMM	SM
SCA1	$Tb(\tau_{SCA}, \omega_{0.05}, \varepsilon_M)$	SCA	0.05	[39]	In-situ
SCA2	$Tb(\tau_{SCA}, \omega_{var}, \varepsilon_M)$		Variational		
DCA1	$Tb(\tau_{DCA}, \omega_{0.05}, \varepsilon_M)$	DCA	0.05		
DCA2	$Tb(\tau_{DCA}, \omega_{var}, \varepsilon_M)$		Variational		

The standard τ-ω is used for *Tb* simulations with in-situ SM as reference input. In this simulation, the difference between *Tb* simulated and the observed is considered as an error. With the same in-situ SM input, we simulate *Tb* but this time by applying the new parameterization of vegetation scattering albedo, ω_{var}. We evaluate the differences between the newly parameterized, time-varying τ-ω model (SCA2 & DCA2) with the results obtained using the control runs (SCA1 & DCA1). The amount of reduction (SCA2 - SCA1 and DCA2 - DCA1) represents the RTM improvement due to the time-variation of the vegetation scattering albedo, ω_{var}.

3. Data

In-situ soil moisture from the U.S. Surface Climate Observing Reference Networks (USCRN) soil moisture network [41] was used as the input for *Tb* simulations from May to November 2015, which are used as the reference for the comparisons. The USCRN sites and soil moisture networks selected for the investigation are presented in Fig. 9 in Appendix: A are located on croplands (with information of crop type) according to MODIS IGBP land cover classification. The detailed description of the study sites is provided in Table 1.

In the SCA (τ_{SCA}) case, the τ-ω model uses a τ value estimated from the MODIS NDVI data. In the DCA (τ_{DCA}) case, τ is retrieved simultaneously in addition to the SM. In both cases, omega is constant 0.05 for the crop surface type following [42].

For the newly parameterized approach, the *Tb* simulations consider the canopy interaction heterogeneity in the τ-ω model by applying time- and space-variable ω, which is a function of the τ estimated in SCA or DCA. The heterogeneity inclusion in the DCA and SCA will be investigated by comparing the SMAPL2 soil moisture product [43–45] in the specific crop sites over USCRN. Furthermore, the validation SMAP Level 2 Enhanced Passive Soil Moisture Product [18, 46] will be

Preprints (www.preprints.org) | NOT PEER-REVIEWED | Posted: 30 July 2020 doi:10.20944/preprints202007.0717.v1

Peer-reviewed version available at Remote Sens. 2020, 12, 2939; doi:10.3390/rs12182939

performed from 2015 to 2019 presented in Table 2. The detailed description of the validation data with SMAP level 2 products at USCRN validation sites and SMAP Level2 Enhanced Products in core validation sites are provided in Table 6 and Table 7.

4. Results

4.1 New parameterization of ω in the τ-ω model

The parameter γ required in Eq. (11) is determined from temporal average of τ_{SCA} and VIIRS *GVF* measurements over the calibration sites (TERENO, HOBE, REMEDHUS, RISMA) as shown in Fig. 2. The determined γ in this study is 1.12 for the GVF simulation (P-value from Wilcoxon rank sum test is 0.6817, which means our hypothesis is reliable enough).

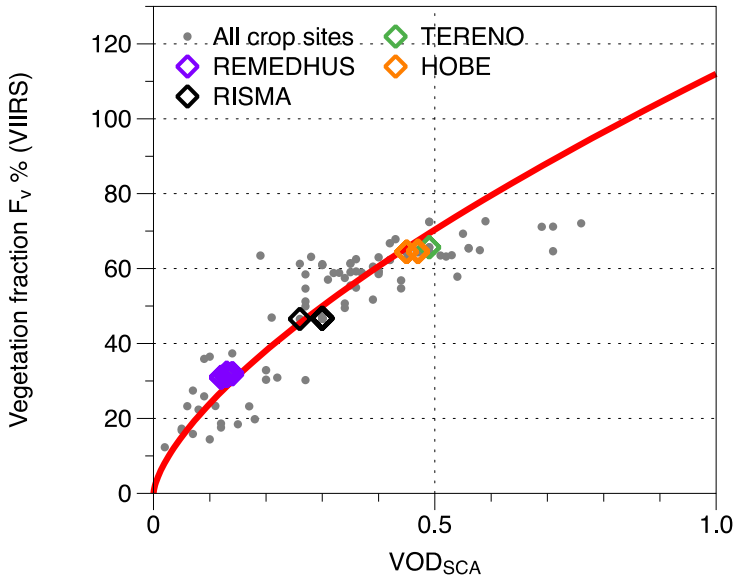

Fig.2 Relationship between vegetation optical depth (VOD-SCA) and the measured vegetation fraction (VIIRS) over croplands.

The computation of the time-varying ω based on Eq. (11) requires also the maximum ω_{max}. For the new parameterization of forward model parameters, the time-varying ω was tuned via the optimal gamma (1.12) and ω_{max}. The results of the calibration and validation are presented in Table 2.

Table 2. Performance of SCA(S) and DCA(D) over the calibration sites (bolds indicate the best)

	Bias				ubRMSE				Correlation			
	S1	S2	D1	D2	S1	S2	D1	D2	S1	S2	D1	D2
TERENO	3.20	**-0.75**	3.37	**0.64**	12.06	**8.49**	9.73	**6.25**	0.91	**0.91**	0.87	**0.91**
HOBE	8.46	**5.90**	2.91	3.77	15.61	**12.23**	**10.48**	11.05	0.86	**0.87**	0.72	**0.74**
RISMA	**-8.38**	-8.69	-6.13	**-4.94**	20.03	**19.72**	14.84	**14.28**	0.49	**0.50**	0.82	**0.82**
REDMUS	-12.04	**-10.94**	-4.44	**-3.70**	37.02	**36.06**	28.93	**28.62**	0.76	**0.76**	**0.78**	0.77

4.2 Quality assessment of the new parameterization in the τ-ω model

We investigate if the τ-ω model error in the simulation of *Tb* is reduced by replacing the time-constant omega ($\omega_{0.05}$) with time-varying omega (ω_{var}) that depends on the value of τ. Eq. (11) indicates that a higher τ measured in a SMAP resolution cell is likely to have a higher effective value of omega;

Higher τ → larger vegetation fraction (less bare soil) in a grid → higher effective ω

Figure 3a shows the significant overestimation of SMAP that SM RTMs can produce. Particularly, the SCA based SM reached the limit value, up to 0.6 m^3/m^3 during half of the time-series. These errors (Fig. 3b) were estimated by deducting in-situ SM and are temporally correlated with the varying ω (Fig. 3c). The SM estimation is affected by the required ancillary parameters of vegetation, τ and ω. If one of the ancillaries is not realistic - in this study the time-constant ω - it will affect the SM estimation. In other words, one of the error sources in SM are the vegetation properties within RTM and this error is at least to a certain extent addressed with time- and space-varying ω. This result confirms the validity of the hypothesis that this ω can be approximated with τ. The τ-derived ω was more than 0.1 and two times larger than the constant ω applied in SMAP baseline algorithm. We investigated the improvement by applying the time- and space-varying ω. The time series of *Tb* in (Fig. 3d) shows that the overestimated *Tb* (blue) decreases in *Tb* simulations with DMM (red curve). The effect of the new parameterization of ω in the τ-ω model is displayed in Fig. 3e. The application of varying ω significantly reduces the *Tb* bias form SCA1 to SCA2. Over cropland as presented in Fig.3 a, this type of SM bias seems to be more of a serious issue in SCA than DCA–based soil moisture retrievals. We can expect the unrealistically overestimated SM from both approaches will have a positive effect by applying varying ω during the SM estimation process from the measured *Tb*. The SMAP DCA SM estimates in the right panel of (3a) are close to 0.6 cm^3/cm^3 missing the seasonal SM evolution observed in-situ. The time-varying ω ranges between 0.08 and 0.12, which is a much larger value than the default value, 0.05. In addition to the large difference in the absolute value, a temporally varying pattern that exhibits a similar pattern of the SM error due to the constant ω. In this case, the application of the time-varying ω also significantly reduced the overestimation of *Tb*.In

On the other hand, in the Fig. 4, the overestimation of SM by using the constant ω in SMAP RTM is less severe than Fig. 3 showing the limited SM value in all-time series in SCA approach. But in this case SM estimated by SCA is much closer to the in-situ SM than the one by DCA. The SCA τ used in the computation of ω (c) in Fig. 4 are lower than the one in Fig. 3. Still, the DCA τ of Fig. 4 range from 0.8 to 0.12, which is similar to the Fig. 3. With given *TB* and higher τ, the SM is higher in the simultaneous optimal estimation. It means that the DCA τ in Fig. 4c should be lower. Particularly, DCA SM error becomes larger when τ was high in DOY 220-230 and 240 & 280, which leads to DCA-based SM much higher than the in-situ in this period. Probably, the further improvement of DCA approach for simultaneous estimation of τ and SM can be expected in the minimization process finding optimal τ with the temporally varying ω than the constant ω.

As a result, SM estimated by SMAPL2 SCA and DCA was overestimated as shown in Fig 3 and 4 (a). The difference of the SMAP SM to the in-situ in (b) shows the temporal correlation with the changes of the omega in DCA of Fig. 3 and 4. It means that both SCA and DCA approaches suffer from a low value of ω; DCA can detect the temporal changes of vegetation better, which is revealed in its SM error. The improvement in *Tb* simulation is mostly originated from the overall larger value of the new ω in both SCA and DCA and less because of the temporal variance. This uncertainty is attributed to the scattering properties of the τ-ω model which was the reason we replaced the constant ω with the varying ω. The results in Figs. 3 and 4 suggest that the soil moisture estimations using the τ-ω model based on the fixed ω were mostly underestimated and the new ω is on a higher level than the constant one showing reduced bias compared to the measured *Tb*.

Preprints (www.preprints.org) | NOT PEER-REVIEWED | Posted: 30 July 2020 doi:10.20944/preprints202007.0717.v1

Peer-reviewed version available at Remote Sens. 2020, 12, 2939; doi:10.3390/rs12182939

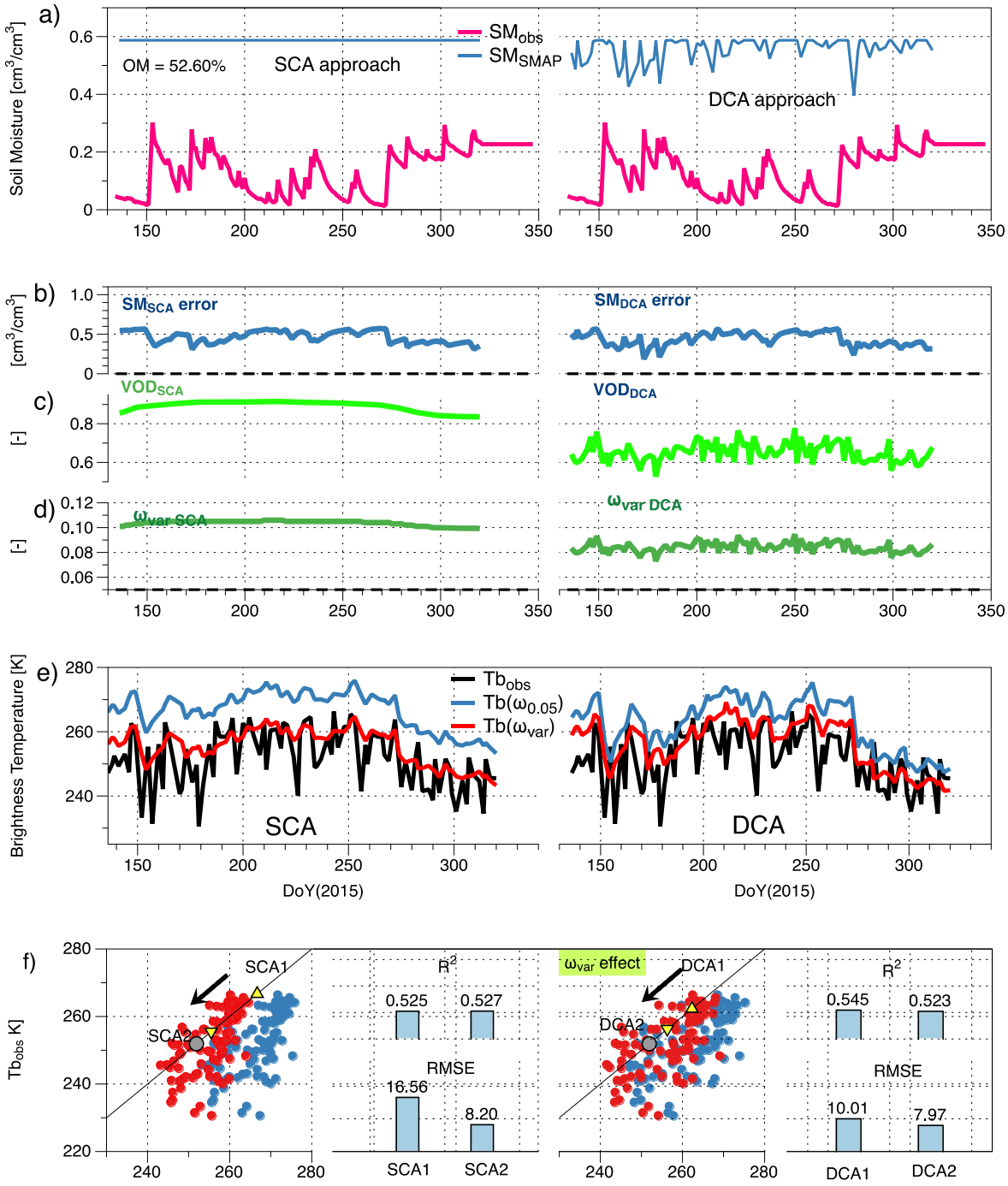

Fig. 3 Validation of the improvement by applying time-varying ω within SCA and DCA approaches; (a) the soil moisture estimation by SCA (left) and DCA (right), (b) their uncertainty, (c) SCA & DCA VOD, (d) the constant adapted by SMAP algorithm and the proposed time-varying ω and (e) the brightness temperature simulated by τ-ω model applied with the constant and time-varying ω from (d) and the input of the in-situ soil moisture presented in (a) in USCRN Durham-2-N (crop type: corn) , (f); ▲: mean SCA&DCA 1,▼: mean SCA&DCA2,● : mean SMAP *Tb* measurements

Preprints (www.preprints.org) | NOT PEER-REVIEWED | Posted: 30 July 2020 doi:10.20944/preprints202007.0717.v1

Peer-reviewed version available at Remote Sens. 2020, 12, 2939; doi:10.3390/rs12182939

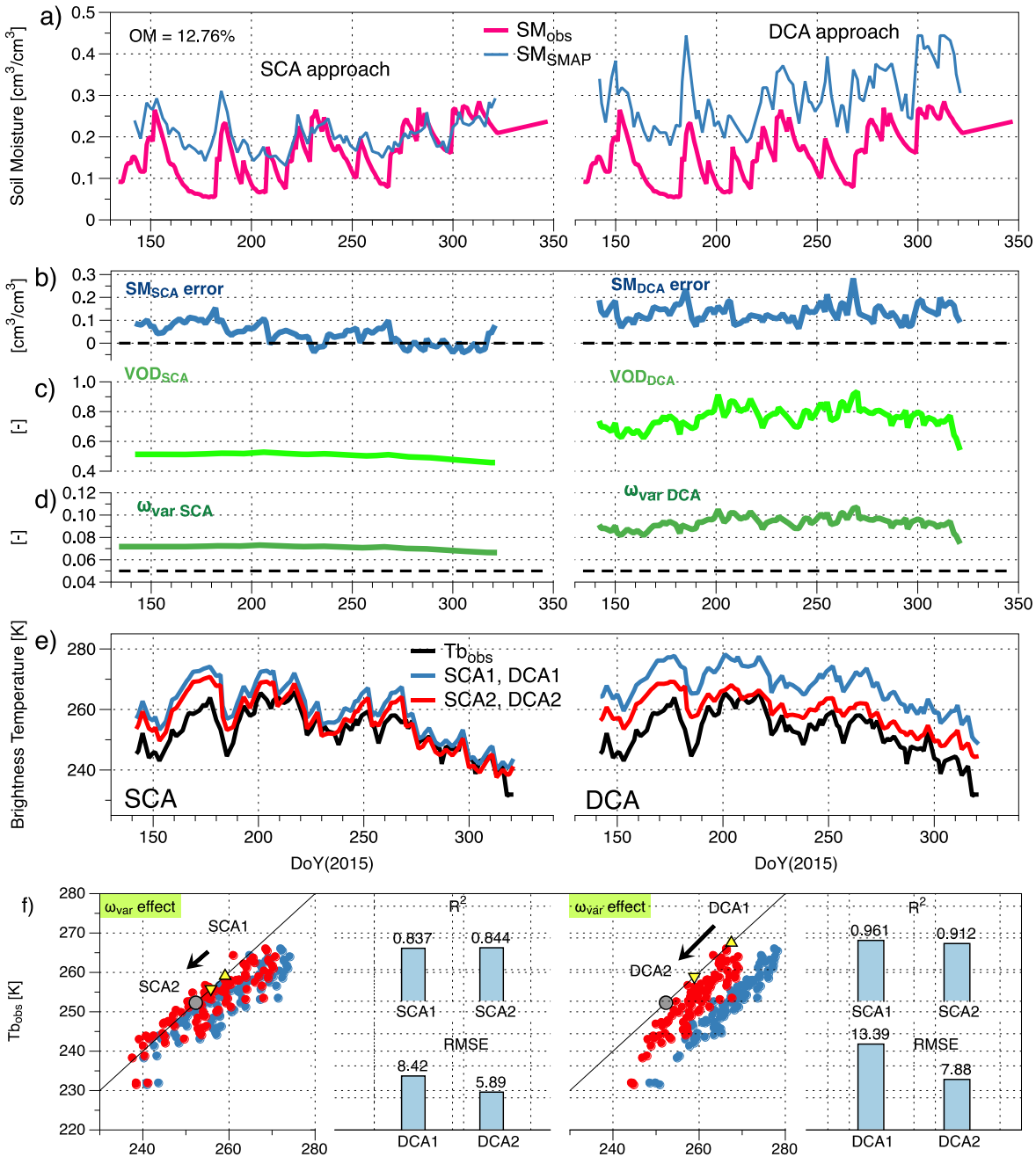

Fig. 4 Validation of the improvement by applying time-varying ω within SCA and DCA approaches; (a) the soil moisture estimation by SCA (left) and DCA (right), (b) their uncertainty, (c) SCA & DCA VOD, (d) the constant adapted by SMAP algorithm and the proposed time-varying ω and (e) the brightness temperature simulated by τ-ω model applied with the constant and time-varying ω from (d) and the input of the in-situ soil moisture presented in (a) in USCRN Gadsden-19-N (crop type: soybean), (f); ▲: mean SCA&DCA 1, ▼: mean SCA&DCA2, ● : mean SMAP *Tb* measurements

During the early growth and senesce period of the crop (soybean), the newly parameterized vegetation ω for cropland in Fig. 5(c) decreases lower than the constant ω (0.05). This dynamic results in reduced SMAP SM estimation. Impacts include: (b) negative bias in SM, (c) low τ in growing and senescence season (d) a lower vegetation ω estimated from the τ.

Preprints (www.preprints.org) | NOT PEER-REVIEWED | Posted: 30 July 2020 doi:10.20944/preprints202007.0717.v1

Peer-reviewed version available at Remote Sens. 2020, 12, 2939; doi:10.3390/rs12182939

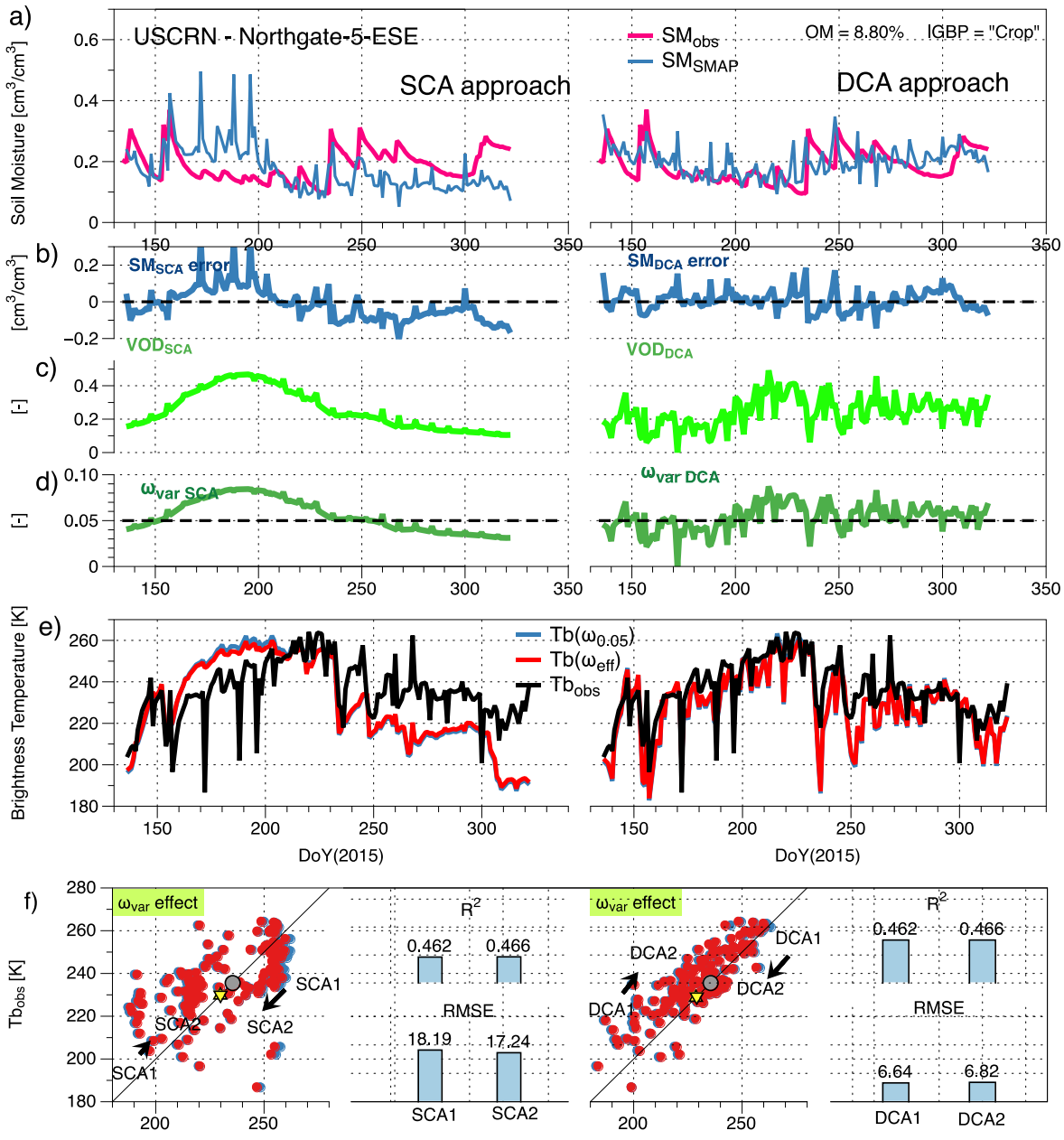

Fig. 5 Validation of the improvement by applying time-varying ω within SCA and DCA approaches; (a) the soil moisture estimation by SCA (left) and DCA (right), (b) their uncertainty, (c) SCA & DCA VOD, (d) the constant adapted by SMAP algorithm and the proposed time-varying ω and (e) the brightness temperature simulated by τ-ω model applied with the constant and time-varying ω from (d) and the input of the in-situ soil moisture presented in (a) in USCRN Northgate-5-ESE (crop type: unknown), (f); ▲: mean SCA&DCA 1, ▼: mean SCA&DCA2, ● : mean SMAP *Tb* measurements

Even though the improvement is not really significant as compared to the case presented in Fig. 3 and 4, the direction of the improvement is promising. The results show an increase of *Tb* simulation when the SMAP SM has a negative bias, which occurs mostly during the growing and ripening season, and decrease of *Tb* simulation when the SMAP SM has a positive bias (similar to the Fig. 3 and 4), which occurs mostly during the mature crop state. The crop phenology shows in the uncertainty (a, b). It appears also in the cause (constant ω) and solution (varying ω) (d) and the improvement (e, f), reasonably. This temporal pattern has been shown not only in the case of USCRN crop case Fig. 5 but also other intensive field studies using SMAP Level 2 Enhanced Passive Soil Moisture [46] over croplands (corn) from 2015 to 2019 in Fig. 6.

Preprints (www.preprints.org) | NOT PEER-REVIEWED | Posted: 30 July 2020 doi:10.20944/preprints202007.0717.v1

Peer-reviewed version available at Remote Sens. 2020, 12, 2939; doi:10.3390/rs12182939

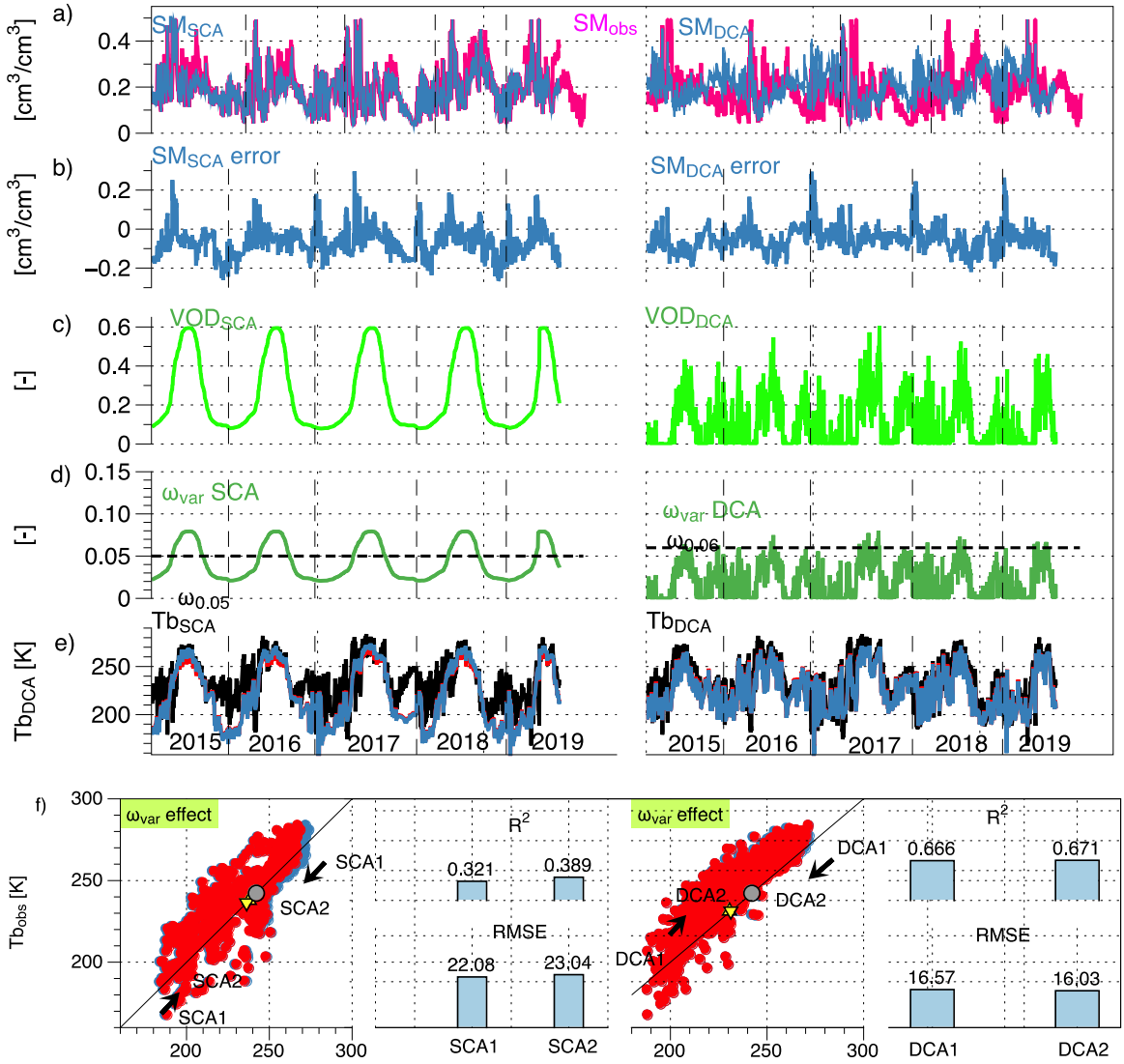

Fig. 6 Validation of the improvement by applying time-varying ω within SCA and DCA approaches; (a) the soil moisture estimation by SCA (left) and DCA (right), (b) their uncertainty, (c) SCA & DCA VOD, (d) the constant adapted by SMAP algorithm and the proposed time-varying ω and (e) the brightness temperature simulated by τ-ω model applied with the constant and time-varying ω from (d) and the input of the in-situ soil moisture presented in (a) in South Fork (crop type: corn) (latitude: 42.42, longitude: -93.41), (f); ▲: mean SCA&DCA 1,▼: mean SCA&DCA2,● : mean SMAP *Tb* measurements

As a result, the vegetation ω variability in the newly parameterized τ-ω model improves the *Tb* simulation. Bias and ubRMSE tend to decrease. Owing to this, the SM estimation from the SMAP *Tb* will be closer to the in-situ SM. Furthermore, the newly parameterized τ-ω model provides a more accurate observation operator for data assimilation, which would result in more accurate soil moisture update to NWP. The validation over the crop sites matched with 9km *Tb* products, showed a very little improvement by varying ω (SCA1→SCA2 and DCA1→DCA2). Further case studies have been performed and the results are summarized in Table 4.

Preprints (www.preprints.org) | NOT PEER-REVIEWED | Posted: 30 July 2020 doi:10.20944/preprints202007.0717.v1

Peer-reviewed version available at Remote Sens. 2020, 12, 2939; doi:10.3390/rs12182939

Table 4. Total validation score over USCRN cropland validation site

	South Fork			Kenaston			Carman		
	bias	ubR	Corr.	bias	ubR	Corr.	bias	ubR	Corr.
SCA1	-7.5	26.2	0.62	**-15.1**	**36.5**	**0.76**	-10.7	25.6	0.82
SCA2	**-7.5**	**25.7**	**0.63**	-15.5	36.7	0.76	**-10.0**	**24.3**	**0.83**
DCA1	-5.41	18.5	0.81	-9.5	22.7	0.85	**0.9**	**8.6**	**0.93**
DCA2	**-4.40**	**17.3**	**0.81**	**-8.7**	**21.4**	**0.85**	1.9	9.3	0.93

*ubR (ubRMSE), the stressed values indicate better score.

Overall, the biases were reduced (SCA1→SCA2 and DCA1→DCA2) and ubRMSE becomes closer to zero for croplands as shown in Table 5 and Fig. 7.

Table 5. Total validation score for USCRN cropland validation site

	Bias				ubRMSE				Correlation			
#	S1	S2	D1	D2	S1	S2	D1	D2	S1	S2	D1	D2
total	**2.9**	0.6	3.7	**2.4**	23.1	**19.5**	21.3	**18.1**	0.725	**0.732**	**0.836**	0.832
win	5	**22**	9	**18**	5	**22**	8	**17**	9	**18**	**15**	12

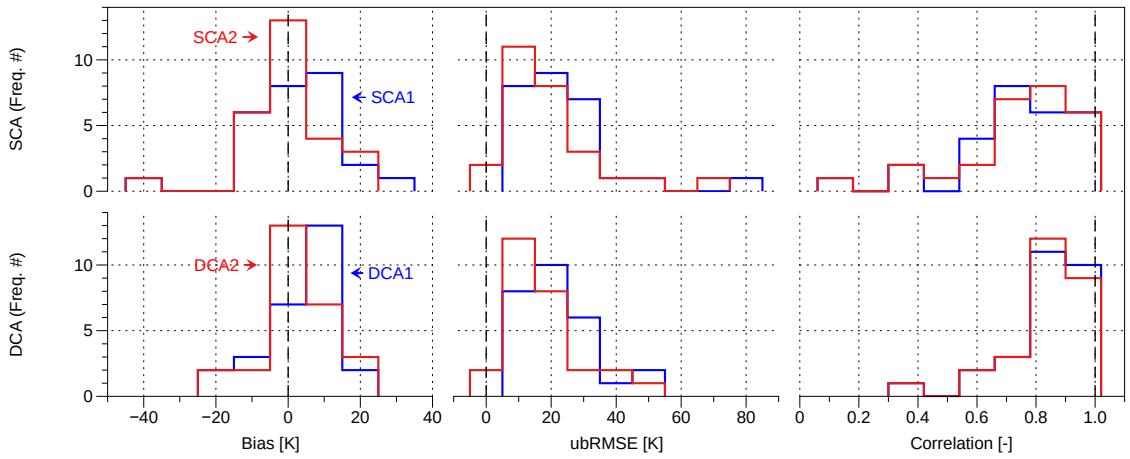

Fig 7. Histogram analysis of bias, ubRMSE and correlation for τ-ω (SCA1&DCA1) and semi-empirical τ-ω (SCA2&DCA2)

More details on the validation statistics for the sites used in Fig.8 can be found in Table 8 of the supplement results in the end of the manuscript.

5. Summary and discussions

In this study, we found that the soil moisture estimated with SCA and DCA from the SMAP mission suffers from over- and under-estimations for cropland sites. In order to tackle this bias, we derived a varying omega (ω_{var}) based on the assumption of a power law relationship between *GVF* and VOD instead of a time-constant omega ($\omega_{0.05}$) used in the SMAP baseline algorithms (SCA and DCA). The formulation allows us to express a time-varying omega ω_{var} based on the dynamics of τ. Hence, ω_{var} is able to account at least partly for the temporal variation of the vegetation properties in cropland. In this study, we focused on linking the measured VOD and the effective value of omega (effective single scattering albedo) mainly via vegetation volumetric traits such as the height and area fraction within the measured resolution cell.

The assessment was performed with the SMAPL2 brightness temperature (*Tb*). It is matched with the forward modelled brightness temperature using in-situ stations of the USCRN (27 croplands (11 corn, 7 soybean, 2 cotton, grapes, alfalfa, 1 wheat, citrus, unknown sites)) in 2015 and in the SMAPL2 Enhanced H-pol brightness core validation sites (3 cropland) from 2015 to 2019. As a result,

we were able to reduce the positive *Tb* bias for several reference sites over cropland (C1, 3-11, 13-17, 20, 22, 25, 27 d in Table 8) including Gadsden-19-N (Atlanta) and Durham-2-N (Boston) presented in the figures 3 and 4. This bias reduction mitigates the overestimation of *Tb* (K) by 80% and 35% in the SCA and DCA approach, respectively. These results demonstrate that owing to a different phenology of the VOD time series over cropland, the time-varying omega parametrized with the VOD can implement more realistic τ - ω model than the one applied with the constant omega.

In a future study, further experiments will be performed including organic matter (OM) to the applied dielectric mixing model [46]. The soil moisture of USCRN used for validation are also estimated from dielectric constant measurement [47], where the soil organic matter is not considered. We assume that this missing consideration in the reference soil moisture values might affect the validation of *Tb* simulations.

As satellite remote sensing is the only operational way to determine global soil moisture, an accurate radiative transfer model is essential. We propose that the presented parameterization for a time-varying vegetation scattering albedo from VOD dynamics implemented within the τ-ω model provides more realistic retrievals of soil moisture dynamics. The key feature of the approach is that no more variables are added with this new parameterization of the τ-ω model contributing to a more accurate but less complex global soil moisture estimation. This is equally important for retrieval and data assimilation approaches based on microwave brightness temperature measurements from SMOS and AMSR-2.

Acknowledgments: The authors specially thank Dr. Howard J. Diamond for providing the data of soil properties over USCRN sites and his valuable advices for this study. This work was funded by the Korea Meteorological Administration Research and Development Program "Development of Climate Prediction System" under Grant (KMA2018-00322). A partial contribution to this work was made at the Jet Propulsion Laboratory, California Institute of Technology under a contract with the National Aeronautics and Space Administration. USDA is an equal opportunity employer and provider.

Appendix A: DATA DESCRIPTION

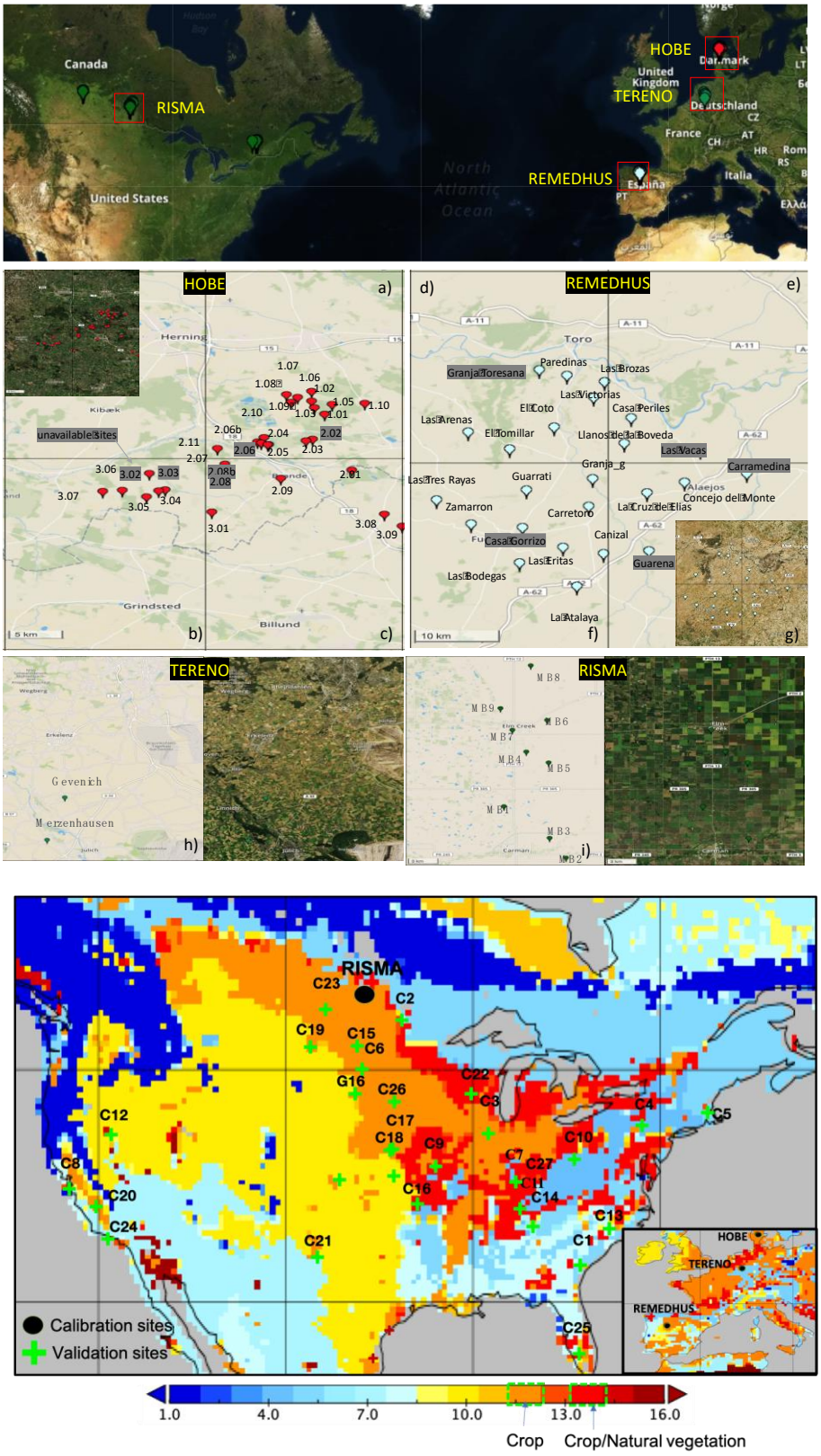

Fig.9 Map of ISMN sites [49] for calibration (upper panel) and validation in USCRN sites (lower panel) over the IGBP land classification based on MODIS measurements obtained from SMAP L4: (orange (IGBP 12): Croplands and red (IGBP 14): Cropland/natural vegetation)

Preprints (www.preprints.org) | NOT PEER-REVIEWED | Posted: 30 July 2020 doi:10.20944/preprints202007.0717.v1

Peer-reviewed version available at Remote Sens. 2020, 12, 2939; doi:10.3390/rs12182939

Table 6. Data used for *Tb* calibration (upper) and validation (lower) over croplands

Calibration Sites	Crop site	Clay [cm3/cm3]	Sand [cm3/cm3]	Silt [cm3/cm3]	OM (%)
HOBE [50]	1.02	0.04	0.87	0.09	27.86
	1.03	0.04	0.87	0.09	27.86
	1.05	0.04	0.87	0.09	27.86
	1.06	0.04	0.87	0.09	27.86
	1.07	0.04	0.87	0.09	27.86
	1.08	0.04	0.87	0.09	27.86
	1.09	0.04	0.87	0.09	27.86
	1.10	0.04	0.87	0.09	27.86
	2.01	0.04	0.87	0.09	28.03
	2.03	0.04	0.87	0.09	28.03
	2.04	0.04	0.87	0.09	28.03
	2.05	0.04	0.87	0.09	28.03
	2.06b	0.04	0.87	0.09	28.03
	2.07	0.04	0.87	0.09	28.03
	2.09	0.04	0.87	0.09	28.03
	2.10	0.04	0.87	0.09	28.03
	2.11	0.04	0.87	0.09	28.03
	3.01	0.04	0.87	0.09	28.03
	3.04	0.04	0.87	0.09	28.03
	3.05	0.04	0.87	0.09	28.03
	3.06	0.04	0.87	0.09	28.03
	3.07	0.04	0.87	0.09	28.03
	3.08	0.1	0.81	0.09	27.62
	3.09	0.1	0.81	0.09	27.62
REMEDHUS [51]	Canizal	0.49	0.19	0.32	2.95
	Carretoro	0.18	0.34	0.48	3.12
	CasaPeriles	0.21	0.36	0.43	3.12
	ConcejodelMonte	0.21	0.36	0.43	3.62
	ElCoto	0.18	0.34	0.48	3.12
	ElTomillar	0.49	0.19	0.32	3.12
	Guarrati	0.18	0.34	0.48	3.12
	LaAtalaya	0.49	0.19	0.32	2.95
	LaCruzdeElias	0.49	0.19	0.32	3.12
	LasArenas	0.49	0.19	0.32	3.38
	LasBodegas	0.21	0.36	0.43	2.95
	LasBrozas	0.49	0.19	0.32	3.12
	LasEritas	0.49	0.19	0.32	2.95
	LasTresRayas	0.49	0.19	0.32	3.38
	LasVictorias	0.49	0.19	0.32	3.12
	LlanosdelaBoveda	0.21	0.36	0.43	3.12
	Paredinas	0.21	0.36	0.43	3.12
	Zamarron	0.49	0.19	0.32	4.36
TERENO [52]	Gevenich	0.22	0.41	0.37	15.13
	Merzenhausen	0.22	0.41	0.37	15.13
RISMA [53]	MB1	0.41	0.12	0.47	13.59
	MB2	0.41	0.12	0.47	11.25
	MB3	0.41	0.12	0.47	14.28
	MB4	0.41	0.12	0.47	14.28
	MB5	0.41	0.12	0.47	14.28
	MB6	0.41	0.12	0.47	14.28
	MB7	0.41	0.12	0.47	13.59
	MB8	0.41	0.12	0.47	15.68
	MB9	0.41	0.12	0.47	13.58

Validation Sites	ID	Clay [cm3/cm3]	Sand [cm3/cm3]	Silt [cm3/cm3]	OM (%)	Crop type
Blackville-3-W	C1	0.23	0.47	0.3	16.33	Cotton
Goodridge-12-NNW	C2	0.22	0.38	0.4	18.42	Soybean
Shabbona-5-NNE	C3	0.24	0.35	0.41	8.47	Corn
Ithaca-13-E	C4	0.2	0.41	0.39	40.15	Corn
Kingston-1-NW	C5	0.05	0.85	0.1	55.06	Corn
Aberdeen-35-WNW	C6	0.23	0.36	0.41	5.76	Corn
Bedford-5-WNW	C7	0.24	0.49	0.27	14.41	Soybean*
Bodega-6-WSW	C8	0.23	0.39	0.38	0.00	Grapes
Chillicothe-22-ENE	C9	0.24	0.35	0.41	7.37	Soybean
Coshocton-8-NNE	C10	0.2	0.41	0.39	18.11	Corn
Crossville-7-NW	C11	0.24	0.49	0.27	16.69	Corn
Denio-52-WSW	C12	0.23	0.36	0.41	3.39	Alfalfa
Durham-2-N	C13	0.13	0.49	0.38	52.60	Corn
Gadsden-19-N	C14	0.24	0.49	0.27	12.76	Soybean
Jamestown-38-WSW	C15	0.09	0.72	0.19	7.88	Soybean
Joplin-24-N	C16	0.24	0.35	0.41	13.52	Soybean*
Lincoln-11-SW	C17	0.24	0.35	0.41	3.91	Corn*
Lincoln-8-ENE	C18	0.24	0.35	0.41	2.72	Corn*
Medora-7-E	C19	0.22	0.43	0.35	5.04	Wheat
Merced-23-WSW	C20	0.2	0.39	0.41	7.57	Alfalfa
Muleshoe-19-S	C21	0.21	0.5	0.29	1.13	Cotton
Necedah-5-WNW	C22	0.06	0.83	0.11	19.47	Corn
Northgate-5-ESE	C23	0.23	0.36	0.41	8.80	-
Santa-Barbara-11-W	C24	0.24	0.47	0.29	0.00	Grapes
Sebring-23-SSE	C25	0.08	0.82	0.1	27.59	citrus
Sioux-Falls-14-NNE	C26	0.23	0.39	0.38	3.82	Corn*
Versailles-3-NNW	C27	0.24	0.47	0.29	14.43	Soybean

The crop type information was extracted from the 30m resolution Cropland Data Layer database [54] within SMAP's 36km grid boundaries for the year 2015 (*: both corn and soybean are dominated within the SMAP grid).

Appendix B: VALIDATION RESULTS

Table 7. Data used for *Tb* validation with SMAPL2 Enhanced H-pol brightness temperature

Site name	State, Country	PI(s)	Land cover	# of senseors	References
South Fork	IA, USA	Cosh	Cropland (corn)	20	[55]
Kenaston	Saskatchewan , Canada	Berg, Rowlandson	cropland	28	[56]
Carman	Manitoba, Canada	McNairn, Pacheco	cropland	9	[53]

Table 8. Validation scores over USCRN cropland

#	Bias				ubRMSE				Correlation			
	S1	S2	D1	D2	S1	S2	D1	D2	S1	S2	D1	D2
C1	11.5	**7.1**	13.8	**9.3**	23.34	**14.63**	27.72	**q**	0.972	**0.971**	**0.985**	0.967
C2	-6.5	**-6.2**	-3.6	**-2.6**	25.25	**24.47**	10.20	**8.76**	0.065	**0.099**	0.932	**0.932**
C3	13.6	**11.8**	-7.2	**-6.5**	31.54	**28.92**	21.88	**20.35**	**0.568**	0.496	0.546	**0.579**
C4	4.5	**-0.6**	5.5	**1.8**	9.6	**3.5**	11.45	**4.47**	0.932	**0.933**	0.960	**0.972**
C5	2.3	**-0.9**	8.8	**-2.8**	19.53	**5.63**	17.99	**6.46**	0.58	**0.79**	**0.806**	0.801
C6	9.9	**9.9**	**7.3**	8.6	**22.72**	22.51	**17.28**	19.46	0.768	**0.782**	**0.890**	0.888
C7	5.3	**0.4**	7.7	**3.9**	11.52	**4.44**	15.71	**8.60**	0.908	**0.915**	0.957	**0.959**
C8	**0.0**	-5.4	-3.2	**-2.6**	**19.88**	22.66	20.39	**20.24**	**0.340**	0.333	**Z**	0.348
C9	5.9	**3.9**	**-0.5**	0.5	14.29	**10.73**	8.55	**8.13**	0.883	**0.896**	0.885	**0.889**
C10	4.8	**0.3**	9.2	**5.4**	10.86	**5.37**	19.08	**11.88**	**0.871**	0.832	0.891	**0.893**
C11	5.1	**-2.4**	9.2	**-0.1**	10.67	**5.55**	18.53	**2.41**	**0.948**	0.947	0.962	**0.968**
C12	-10.7	**-10.0**	**2.4**	2.7	25.45	**24.28**	**13.18**	13.28	0.682	**0.684**	0.738	**0.746**
C13	14.9	**3.9**	6.5	**2.3**	30.71	**10.69**	15.14	**8.97**	0.724	**0.725**	**0.738**	0.723
C14	7.2	**4.0**	13.2	**7.0**	15.12	**9.15**	26.50	**14.48**	**0.918**	0.915	**0.980**	0.955
C15	15.2	**15.2**	**14.4**	15.5	32.49	**32.23**	**29.89**	32.00	0.744	**0.757**	**0.904**	0.900
C16	1.4	**0.8**	-1.7	**-0.8**	8.82	**8.38**	10.75	**9.92**	0.913	**0.920**	**0.900**	0.899
C17	0.4	**-0.0**	-5.8	**-4.5**	12.65	**12.19**	17.67	**16.37**	0.812	**0.815**	**0.872**	0.871
C18	**-1.2**	-2.1	-12.7	**-11.4**	**15.00**	15.03	27.10	**24.67**	0.691	**0.695**	0.900	**0.902**
C19	-5.4	**-4.4**	**5.8**	7.2	16.12	**14.84**	**14.51**	16.87	0.582	**0.589**	0.787	**0.788**
C20	**17.3**	18.0	**20.6**	21.9	**36.27**	37.64	**42.48**	44.95	0.853	**0.853**	0.884	**0.887**
C21	-37.7	**-36.6**	-21.5	**-20.8**	76.97	**74.80**	45.03	**43.72**	**0.761**	0.760	**0.825**	0.825
C22	13.6	**8.4**	13.1	**8.8**	27.71	**17.50**	26.63	**18.32**	**0.855**	0.847	**0.895**	0.838
C23	-7.8	**-7.7**	**0.9**	2.2	22.70	**21.82**	**6.85**	7.83	0.680	**0.683**	0.875	**0.876**
C24	**-6.5**	-6.5	**3.8**	4.9	**15.72**	15.82	**10.36**	12.13	0.349	**0.354**	**0.551**	0.545
C25	26.2	**23.9**	**22.6**	23.2	53.64	**49.25**	**46.73**	47.82	0.549	**0.553**	**0.709**	0.687
C26	**-9.0**	-10.2	-16.1	**-15.0**	**26.59**	27.40	34.56	**32.60**	**0.730**	0.724	**0.865**	0.864
C27	2.8	**0.4**	8.7	**6.4**	8.41	**6.36**	18.02	**13.52**	**0.889**	0.883	**0.937**	0.952

References

1. Vitart, F.; Ardilouze, C.; Bonet, A.; Brookshaw, A.; Chen, M.; Codorean, C.; Déqué, M.; Ferranti, L.; Fucile, E.; Fuentes, M.; Hendon, H.; Hodgson, J.; Kang, H.-S.; Kumar, A.; Lin, H.; Liu, G.; Liu, X.; Malguzzi, P.; Mallas, I.; Manoussakis, M.; Mastrangelo, D.; MacLachlan, C.; McLean, P.; Minami, A.; Mladek, R.; Nakazawa, T.; Najm, S.; Nie, Y.; Rixen, M.; Robertson, A. W.; Ruti, P.; Sun, C.; Takaya, Y.; Tolstykh, M.; Venuti, F.; Waliser, D.; Woolnough, S.; Wu, T.; Won, D.-J.; Xiao, H.; Zaripov, R.; Zhang, L. The Subseasonal to Seasonal (S2S) Prediction Project Database. *Bulletin of the American Meteorological Society* **2017**, *98* (1), 163–173. https://doi.org/10.1175/BAMS-D-16-0017.1.
2. Miralles, D. G.; Teuling, A. J.; van Heerwaarden, C. C.; de Arellano, J. V. G. Mega-Heatwave Temperatures Due to Combined Soil Desiccation and Atmospheric Heat Accumulation. *Nature Geoscience* **2014**, *7* (5), 345–349. https://doi.org/10.1038/ngeo2141.
3. Peterson, T. C.; Heim, R. R.; Hirsch, R.; Kaiser, D. P.; Brooks, H.; Diffenbaugh, N. S.; Dole, R. M.; Giovannettone, J. P.; Guirguis, K.; Karl, T. R.; Katz, R. W.; Kunkel, K.; Lettenmaier, D.; McCabe, G. J.; Paciorek, C. J.; Ryberg, K. R.; Schubert, S.; Silva, V. B. S.; Stewart, B. C.; Vecchia, A. v.; Villarini, G.; Vose, R. S.; Walsh, J.; Wehner, M.; Wolock, D.; Wolter, K.; Woodhouse, C. A.; Wuebbles, D. Monitoring

and Understanding Changes in Heat Waves, Cold Waves, Floods, and Droughts in the United States: State of Knowledge. *Bulletin of the American Meteorological Society* **2013**, *94* (6), 821–834. https://doi.org/10.1175/BAMS-D-12-00066.1.

4. Mariotti, A.; Ruti, P. M.; Rixen, M. Progress in Subseasonal to Seasonal Prediction through a Joint Weather and Climate Community Effort. *npj Climate and Atmospheric Science* **2018**, *1* (1), 1–4. https://doi.org/10.1038/s41612-018-0014-z.
5. Yoon, J.-H.; Leung, L. R. Assessing the Relative Influence of Surface Soil Moisture and ENSO SST on Precipitation Predictability over the Contiguous United States. *Geophysical Research Letters* **2015**, *42* (12), 5005–5013. https://doi.org/10.1002/2015GL064139.
6. Santanello, J. A.; Dirmeyer, P. A.; Ferguson, C. R.; Findell, K. L.; Tawfik, A. B.; Berg, A.; Ek, M.; Gentine, P.; Guillod, B. P.; van Heerwaarden, C.; Roundy, J.; Wulfmeyer, V. Land-Atmosphere Interactions the LoCo Perspective. *Bulletin of the American Meteorological Society*. American Meteorological Society June 1, 2018, pp 1253–1272. https://doi.org/10.1175/BAMS-D-17-0001.1.
7. Santanello Jr., J. A.; Lawston, P.; Kumar, S.; Dennis, E. Understanding the Impacts of Soil Moisture Initial Conditions on NWP in the Context of Land–Atmosphere Coupling. *Journal of Hydrometeorology* **2019**, *20* (5), 793–819. https://doi.org/10.1175/JHM-D-18-0186.1.
8. Reichle, R. H.; Koster, R. D.; Dong, J.; Berg, A. A.; Reichle, R. H.; Koster, R. D.; Dong, J.; Berg, A. A. Global Soil Moisture from Satellite Observations, Land Surface Models, and Ground Data: Implications for Data Assimilation. *http://dx.doi.org/10.1175/1525-7541(2004)005<0430:GSMFSO>2.0.CO;2* **2004**.
9. Reichle, R. H.; de Lannoy, G. J. M.; Liu, Q.; Koster, R. D.; Kimball, J. S.; Crow, W. T.; Ardizzone, J. v.; Chakraborty, P.; Collins, D. W.; Conaty, A. L.; Girotto, M.; Jones, L. A.; Kolassa, J.; Lievens, H.; Lucchesi, R. A.; Smith, E. B. Global Assessment of the SMAP Level-4 Surface and Root-Zone Soil Moisture Product Using Assimilation Diagnostics. *Journal of Hydrometeorology* **2017**, *18* (12), 3217–3237. https://doi.org/10.1175/JHM-D-17-0130.1.
10. Reichle, R. H.; de Lannoy, G. J. M.; Liu, Q.; Ardizzone, J. v.; Chen, F.; Colliander, A.; Conaty, A.; Crow, W.; Jackson, T.; Kimball, J.; Koster, R. D.; Smith, E. B. *Global Modeling and Assimilation Office Soil Moisture Active Passive Mission L4_SM Data Product Assessment (Version 2 Validated Release)*; 2016.
11. Reichle, R. H.; Ardizzone, J. v.; Kim, G.-K.; Lucchesi, R. A.; Smith, E. B.; Weiss, B. H. *Global Modeling and Assimilation Office Soil Moisture Active Passive (SMAP) Mission Level 4 Surface and Root Zone Soil Moisture (L4_SM) Product Specification Document*; 2018.
12. de Lannoy, G. J. M.; Reichle, R. H. Assimilation of SMOS Brightness Temperatures or Soil Moisture Retrievals into a Land Surface Model. *Hydrology and Earth System Sciences* **2016**, *20* (12), 4895–4911. https://doi.org/10.5194/hess-20-4895-2016.
13. de Lannoy, G. J. M.; Reichle, R. H. Global Assimilation of Multiangle and Multipolarization SMOS Brightness Temperature Observations into the GEOS-5 Catchment Land Surface Model for Soil Moisture Estimation. *Journal of Hydrometeorology* **2016**, *17* (2), 669–691. https://doi.org/10.1175/JHM-D-15-0037.1.
14. de Rosnay, P.; Calvet, J. C.; Kerr, Y.; Wigneron, J. P.; Lemaître, F.; Escorihuela, M. J.; Sabater, J. M.; Saleh, K.; Barrié, J.; Bouhours, G.; Coret, L.; Cherel, G.; Dedieu, G.; Durbe, R.; Fritz, N. E. D.; Froissard, F.; Hoedjes, J.; Kruszewski, A.; Lavenu, F.; Suquia, D.; Waldteufel, P. SMOSREX: A Long Term Field Campaign Experiment for Soil Moisture and Land Surface Processes Remote Sensing. *Remote Sensing of Environment* **2006**, *102* (3–4), 377–389. https://doi.org/10.1016/j.rse.2006.02.021.
15. Jackson, T. J.; Schmugge, J.; Engman, E. T. Application de La Télédétection à l'hydrologie: L'humidité Du Sol. *Hydrological Sciences Journal* **1996**, *41* (4), 517–530. https://doi.org/10.1080/02626669609491523.
16. Wigneron, J. P.; Calvet, J. C.; Pellarin, T.; van de Griend, A. A.; Berger, M.; Ferrazzoli, P. Retrieving Near-Surface Soil Moisture from Microwave Radiometric Observations: Current Status and Future Plans. *Remote Sensing of Environment*. Elsevier Inc. June 15, 2003, pp 489–506. https://doi.org/10.1016/S0034-4257(03)00051-8.
17. Mo, T.; Choudhury, B. J.; Schmugge, T. J.; Wang, J. R.; Jackson, T. J. A Model for Microwave Emission from Vegetation-Covered Fields. *Journal of Geophysical Research* **1982**, *87* (C13), 11229. https://doi.org/10.1029/JC087iC13p11229.
18. Chan, S. K.; Bindlish, R.; O'Neill, P.; Jackson, T.; Njoku, E.; Dunbar, S.; Chaubell, J.; Piepmeier, J.; Yueh, S.; Entekhabi, D.; Colliander, A.; Chen, F.; Cosh, M. H.; Caldwell, T.; Walker, J.; Berg, A.; McNairn, H.; Thibeault, M.; Martínez-Fernández, J.; Uldall, F.; Seyfried, M.; Bosch, D.; Starks, P.; Holifield Collins, C.; Prueger, J.; van der Velde, R.; Asanuma, J.; Palecki, M.; Small, E. E.; Zreda, M.; Calvet, J.; Crow, W. T.; Kerr, Y. Development and Assessment of the SMAP Enhanced Passive Soil Moisture Product. *Remote Sensing of Environment* **2018**, *204*, 931–941. https://doi.org/10.1016/j.rse.2017.08.025.

19. Rodríguez-Fernández, N. J.; Mialon, A.; Mermoz, S.; Bouvet, A.; Richaume, P.; al Bitar, A.; Al-Yaari, A.; Brandt, M.; Kaminski, T.; le Toan, T.; Kerr, Y. H.; Wigneron, J. P. An Evaluation of SMOS L-Band Vegetation Optical Depth (L-VOD) Data Sets: High Sensitivity of L-VOD to above-Ground Biomass in Africa. *Biogeosciences* **2018**, *15* (14), 4627–4645. https://doi.org/10.5194/bg-15-4627-2018.
20. Owe, M.; de Jeu, R.; Walker, J. A Methodology for Surface Soil Moisture and Vegetation Optical Depth Retrieval Using the Microwave Polarization Difference Index. *IEEE Transactions on Geoscience and Remote Sensing* **2001**, *39* (8), 1643–1654. https://doi.org/10.1109/36.942542.
21. Konings, A. G.; Piles, M.; Rötzer, K.; McColl, K. A.; Chan, S. K.; Entekhabi, D. Vegetation Optical Depth and Scattering Albedo Retrieval Using Time Series of Dual-Polarized L-Band Radiometer Observations. *Remote Sensing of Environment* **2016**, *172*, 178–189. https://doi.org/10.1016/j.rse.2015.11.009.
22. Zwieback, S., Colliander, A., Cosh, M.H., Martínez-Fernándezj, J., McNairn, H., Starks, P.J., Thibeault, M. and Berg, A., 2018. Estimating time-dependent vegetation biases in the SMAP soil moisture product. Hydrology and Earth System Sciences, 22(8), pp.4473-4489.
23. Jackson, T. J.; Schmugge, T. J. Vegetation Effects on the Microwave Emission of Soils. Remote Sensing of Environment 1991, 36 (3), 203–212. https://doi.org/10.1016/0034-4257(91)90057-D.
24. Konings, A. G.; Piles, M.; Das, N.; Entekhabi, D. L-Band Vegetation Optical Depth and Effective Scattering Albedo Estimation from SMAP. *Remote Sensing of Environment* **2017**, *198*, 460–470. https://doi.org/10.1016/j.rse.2017.06.037.
25. Jiang, L.; Kogan, F. N.; Guo, W.; Tarpley, J. D.; Mitchell, K. E.; Ek, M. B.; Tian, Y.; Zheng, W.; Zou, C.-Z.; Ramsay, B. H. Real-Time Weekly Global Green Vegetation Fraction Derived from Advanced Very High Resolution Radiometer-Based NOAA Operational Global Vegetation Index (GVI) System. *Journal of Geophysical Research* **2010**, *115* (D11), D11114. https://doi.org/10.1029/2009JD013204.
26. Asner, G. P.; Mascaro, J.; Anderson, C.; Knapp, D. E.; Martin, R. E.; Kennedy-Bowdoin, T.; van Breugel, M.; Davies, S.; Hall, J. S.; Muller-Landau, H. C.; Potvin, C.; Sousa, W.; Wright, J.; Bermingham, E. High-Fidelity National Carbon Mapping for Resource Management and REDD+. *Carbon Balance and Management* **2013**, *8* (1), 1–14. https://doi.org/10.1186/1750-0680-8-7.
27. Asner, G. P.; Mascaro, J. Mapping Tropical Forest Carbon: Calibrating Plot Estimates to a Simple LiDAR Metric. *Remote Sensing of Environment* **2014**, *140*, 614–624. https://doi.org/10.1016/j.rse.2013.09.023.
28. Chave, J.; Réjou-Méchain, M.; Búrquez, A.; Chidumayo, E.; Colgan, M. S.; Delitti, W. B. C.; Duque, A.; Eid, T.; Fearnside, P. M.; Goodman, R. C.; Henry, M.; Martínez-Yrízar, A.; Mugasha, W. A.; Muller-Landau, H. C.; Mencuccini, M.; Nelson, B. W.; Ngomanda, A.; Nogueira, E. M.; Ortiz-Malavassi, E.; Pélissier, R.; Ploton, P.; Ryan, C. M.; Saldarriaga, J. G.; Vieilledent, G. Improved Allometric Models to Estimate the Aboveground Biomass of Tropical Trees. *Global Change Biology* **2014**, *20* (10), 3177–3190. https://doi.org/10.1111/gcb.12629.
29. Chambers, J. Q.; Santos, J. dos; Ribeiro, R. J.; Higuchi, N. Tree Damage, Allometric Relationships, and above-Ground Net Primary Production in Central Amazon Forest. *Forest Ecology and Management* **2001**, *152* (1–3), 73–84. https://doi.org/10.1016/S0378-1127(00)00591-0.
30. Chave, J.; Andalo, C.; Brown, S.; Cairns, M. A.; Chambers, J. Q.; Eamus, D.; Fölster, H.; Fromard, F.; Higuchi, N.; Kira, T.; Lescure, J. P.; Nelson, B. W.; Ogawa, H.; Puig, H.; Riéra, B.; Yamakura, T. Tree Allometry and Improved Estimation of Carbon Stocks and Balance in Tropical Forests. *Oecologia* **2005**, *145* (1), 87–99. https://doi.org/10.1007/s00442-005-0100-x.
31. Jagdhuber, T.; Konings, A. G.; McColl, K. A.; Alemohammad, S. H.; Das, N. N.; Montzka, C.; Link, M.; Akbar, R.; Entekhabi, D. Physics-Based Modeling of Active and Passive Microwave Covariations over Vegetated Surfaces. *IEEE Transactions on Geoscience and Remote Sensing* **2019**, *57* (2), 788–802. https://doi.org/10.1109/TGRS.2018.2860630.
32. Norman, J. M.; Kustas, W. P.; Humes, K. S. Source Approach for Estimating Soil and Vegetation Energy Fluxes in Observations of Directional Radiometric Surface Temperature [Agric. For. Meteorol., 77 (1995) 263–293]. *Agricultural and Forest Meteorology* **1996**, *80* (2–4), 297. https://doi.org/10.1016/0168-1923(96)02344-1.
33. Rodríguez-Fernández, N. J.; Mialon, A.; Mermoz, S.; Bouvet, A.; Richaume, P.; al Bitar, A.; Al-Yaari, A.; Brandt, M.; Kaminski, T.; le Toan, T.; Kerr, Y. H.; Wigneron, J.-P. An Evaluation of SMOS L-Band Vegetation Optical Depth (L-VOD) Data Sets: High Sensitivity of L-VOD to above-Ground Biomass in Africa. *Biogeosciences* **2018**, *15* (14), 4627–4645. https://doi.org/10.5194/bg-15-4627-2018.
34. Chaubell, M. J.; Asanuma, J.; Berg, A. A.; Bosch, D. D.; Caldwell, T.; Cosh, M. H.; Collins, C. H.; Martinez-Fernandez, J.; Seyfried, M.; Starks, P. J.; Su, Z.; Yueh, S. H.; Thibeault, M.; Walker, J.; Dunbar, R. S.; Colliander, A.; Chen, F.; Chan, S. K.; Entekhabi, D.; Bindlish, R.; O'Neill, P. E. Improved SMAP

Dual-Channel Algorithm for the Retrieval of Soil Moisture. *IEEE Transactions on Geoscience and Remote Sensing* **2020**, 1–12. https://doi.org/10.1109/tgrs.2019.2959239.

35. Fernandez-Moran, R.; Wigneron, J. P.; Lopez-Baeza, E.; Al-Yaari, A.; Coll-Pajaron, A.; Mialon, A.; Miernecki, M.; Parrens, M.; Salgado-Hernanz, P. M.; Schwank, M.; Wang, S.; Kerr, Y. H. Roughness and Vegetation Parameterizations at L-Band for Soil Moisture Retrievals over a Vineyard Field. *Remote Sensing of Environment* **2015**, *170*, 269–279. https://doi.org/10.1016/j.rse.2015.09.006.
36. Fernandez-Moran, R.; Al-Yaari, A.; Mialon, A.; Mahmoodi, A.; al Bitar, A.; de Lannoy, G.; Rodriguez-Fernandez, N.; Lopez-Baeza, E.; Kerr, Y.; Wigneron, J.-P. SMOS-IC: An Alternative SMOS Soil Moisture and Vegetation Optical Depth Product. *Remote Sensing* **2017**, *9* (5), 457. https://doi.org/10.3390/rs9050457.
37. Pellarin, T.; Wigneron, J. P.; Calvet, J. C.; Waldteufel, P. Global Soil Moisture Retrieval from a Synthetic L-Band Brightness Temperature Data Set. *Journal of Geophysical Research Atmospheres* **2003**, *108* (12). https://doi.org/10.1029/2002jd003086.
38. Pellarin, T.; Tran, T.; Cohard, J.-M.; Galle, S.; Laurent, J.-P.; de Rosnay, P.; Vischel, T. Soil Moisture Mapping over West Africa with a 30-Min Temporal Resolution Using AMSR-E Observations and a Satellite-Based Rainfall Product. *Hydrology and Earth System Sciences* **2009**, *13* (10), 1887–1896. https://doi.org/10.5194/hess-13-1887-2009.
39. Wigneron, J.-P.; Pellarin, T.; Calvet, J.-C.; de Rosnay, P.; Saleh, K.; Waldteufel, P.; Kerr, Y. L-MEB: A Simple Model at L-Band for the Continental Areas - Application to the Simulation of a Half-Degree Resolution and Global Scale Dataset. *Thermal microwave radiation: applications for remote sensing.2006, 362-371* **2006**.
40. Park, C.-H.; Behrendt, A.; LeDrew, E.; Wulfmeyer, V. New Approach for Calculating the Effective Dielectric Constant of the Moist Soil for Microwaves. *Remote Sensing* **2017**, *9* (7), 732. https://doi.org/10.3390/rs9070732.
41. Bell, J. E.; Palecki, M. A.; Baker, C. B.; Collins, W. G.; Lawrimore, J. H.; Leeper, R. D.; Hall, M. E.; Kochendorfer, J.; Meyers, T. P.; Wilson, T.; Diamond, H. J. U.S. Climate Reference Network Soil Moisture and Temperature Observations. *Journal of Hydrometeorology* **2013**, *14* (3), 977–988. https://doi.org/10.1175/JHM-D-12-0146.1.
42. Chan, S. K.; Bindlish, R.; O'Neill, P. E.; Njoku, E.; Jackson, T.; Colliander, A.; Chen, F.; Burgin, M.; Dunbar, S.; Piepmeier, J.; Yueh, S.; Entekhabi, D.; Cosh, M. H.; Caldwell, T.; Walker, J.; Wu, X.; Berg, A.; Rowlandson, T.; Pacheco, A.; McNairn, H.; Thibeault, M.; Martinez-Fernandez, J.; Gonzalez-Zamora, A.; Seyfried, M.; Bosch, D.; Starks, P.; Goodrich, D.; Prueger, J.; Palecki, M.; Small, E. E.; Zreda, M.; Calvet, J. C.; Crow, W. T.; Kerr, Y. Assessment of the SMAP Passive Soil Moisture Product. *IEEE Transactions on Geoscience and Remote Sensing* **2016**, *54* (8), 4994–5007. https://doi.org/10.1109/TGRS.2016.2561938.
43. O'Neill, P.; Entekhabi, D.; Njoku, E.; Kellogg, K. The NASA Soil Moisture Active Passive (SMAP) Mission: Overview. In *International Geoscience and Remote Sensing Symposium (IGARSS)*; 2010; pp 3236–3239. https://doi.org/10.1109/IGARSS.2010.5652291.
44. Chan, S. K.; Bindlish, R.; O'Neill, P. E.; Njoku, E.; Jackson, T.; Colliander, A.; Chen, F.; Burgin, M.; Dunbar, S.; Piepmeier, J.; Yueh, S.; Entekhabi, D.; Cosh, M. H.; Caldwell, T.; Walker, J.; Wu, X.; Berg, A.; Rowlandson, T.; Pacheco, A.; McNairn, H.; Thibeault, M.; Martinez-Fernandez, J.; Gonzalez-Zamora, A.; Seyfried, M.; Bosch, D.; Starks, P.; Goodrich, D.; Prueger, J.; Palecki, M.; Small, E. E.; Zreda, M.; Calvet, J. C.; Crow, W. T.; Kerr, Y. Assessment of the SMAP Passive Soil Moisture Product. *IEEE Transactions on Geoscience and Remote Sensing* **2016**, *54* (8), 4994–5007. https://doi.org/10.1109/TGRS.2016.2561938.
45. SMAP L2 Radiometer Half-Orbit 36 km EASE-Grid Soil Moisture, Version 6 | National Snow and Ice Data Center https://nsidc.org/data/SPL2SMP/versions/6 (accessed Jun 4, 2020).
46. Colliander, A.; Jackson, T. J.; Bindlish, R.; Chan, S.; Das, N.; Kim, S. B.; Cosh, M. H.; Dunbar, R. S.; Dang, L.; Pashaian, L.; Asanuma, J.; Aida, K.; Berg, A.; Rowlandson, T.; Bosch, D.; Caldwell, T.; Caylor, K.; Goodrich, D.; al Jassar, H.; Lopez-Baeza, E.; Martínez-Fernández, J.; González-Zamora, A.; Livingston, S.; McNairn, H.; Pacheco, A.; Moghaddam, M.; Montzka, C.; Notarnicola, C.; Niedrist, G.; Pellarin, T.; Prueger, J.; Pulliainen, J.; Rautiainen, K.; Ramos, J.; Seyfried, M.; Starks, P.; Su, Z.; Zeng, Y.; van der Velde, R.; Thibeault, M.; Dorigo, W.; Vreugdenhil, M.; Walker, J. P.; Wu, X.; Monerris, A.; O'Neill, P. E.; Entekhabi, D.; Njoku, E. G.; Yueh, S. Validation of SMAP Surface Soil Moisture Products with Core Validation Sites. *Remote Sensing of Environment* **2017**, *191*, 215–231. https://doi.org/10.1016/j.rse.2017.01.021.

47. Park, C.; Montzka, C.; Jagdhuber, T.; Jonard, F.; de Lannoy, G.; Hong, J.; Jackson, T. J.; Wulfmeyer, V. A Dielectric Mixing Model Accounting for Soil Organic Matter. *Vadose Zone Journal* **2019**, *18* (1), 190036. https://doi.org/10.2136/vzj2019.04.0036.
48. Seyfried, M. S.; Grant, L. E.; Du, E.; Humes, K. Dielectric Loss and Calibration of the Hydra Probe Soil Water Sensor. *Vadose Zone Journal* **2005**, *4* (4), 1070–1079. https://doi.org/10.2136/vzj2004.0148.
49. Dorigo, W.A.; Xaver, A.; Vreugdenhil, M.; Gruber, A.; Hegyiová, A.; Sanchis-Dufau, A.D.; Zamojski, D.; Cordes, C.; Wagner, W.; Drusch, M. Global Automated Quality Control of In Situ Soil Moisture Data from the International Soil Moisture Network. *Vadose Zone Journal* **2012**, *12* (3): vzj2012.0097. doi: https://doi.org/10.2136/vzj2012.0097
50. Bircher, S.; Skou, N.; Jensen, K. H.; Walker, J. P.; Rasmussen, L.; Verhoest, N. A soil moisture and temperature network for SMOS validation in Western Denmark. *Hydrology & Earth System Sciences* **2012**, *16*(5).
51. Sanchez, N.; Martínez-Fernández, J.; Scaini, A.; Perez-Gutierrez, C. Validation of the SMOS L2 soil moisture data in the REMEDHUS network (Spain). *IEEE Transactions on Geoscience and Remote Sensing* **2012**, *50*(5), 1602-1611
52. Bogena, H. R.; Montzka, C.; Huisman, J. A.; Graf, A.; Schmidt, M.; Stockinger, von Hebel C.; Hendricks-Franssen HJ; van der Kruk J; Tappe W.; Lücke A The TERENO-Rur hydrological observatory: A multiscale multi-compartment research platform for the advancement of hydrological science. *Vadose Zone Journal* **2018**, *17*(1), 1-22.
53. Bhuiyan, H.A.; McNairn, H., Powers, J.; Friesen, M.; Pacheco, A.; Jackson, T.J.; Cosh, M.H.; Colliander, A.; Berg, A.; Rowlandson, T.; Bullock, P. 2018. Assessing SMAP soil moisture scaling and retrieval in the Carman (Canada) study site. Vadose Zone Journal, 17(1), pp.1-14.
54. Johnson, D.; R. Mueller. The 2009 Cropland Data Layer Photogrammetric Engineering and Remote Sensing November 2010, pp 1201-1205.
55. Coopersmith, E. J.; Cosh, M. H.; Petersen, W. A.; Prueger, J.; Niemeier, J. J. Soil Moisture Model Calibration and Validation: An ARS Watershed on the South Fork Iowa River. *Journal of Hydrometeorology* **2015**, *16* (3), 1087–1101. https://doi.org/10.1175/JHM-D-14-0145.1.
56. Tetlock, E.; Toth, B.; Berg, A.; Rowlandson, T.; Ambadan, J. T. An 11-Year (2007–2017) Soil Moisture and Precipitation Dataset from the Kenaston Network in the Brightwater Creek Basin, Saskatchewan, Canada. Earth System Science Data 2019, 11 (2), 787–796. https://doi.org/10.5194/essd-11-787-2019.